Characterization of a Silicon-Based Shear-Force Sensor on Human Subjects

Lin Wang and David J. Beebe*, *Member, IEEE*

***Abstract*—A silicon sensor is developed and its ability to measure both compressive and shear forces at the skin–object interface is characterized. The sensor is designed based on the piezoresistive effect and fabricated using integrated circuit and microelectromechanical systems technologies. The sensor utilizes a mesa structure that leads to asymmetric diaphragm deformations in response to nonnormal loading. Four independent ion-implanted piezoresistors are used to detect the stresses induced in diaphragm and resolve both the compressive- and shear-force components. The sensor is calibrated on human subjects over a range of applied force (5- to 40-N shear force at increments of 1.25 N; 0- to 30-N compressive force). Force measurement via a tracking experiment is evaluated at four shear (9, 18, 25, and 35 N) and three compressive (7, 15, and 26 N) force levels. The sensor has good repeatability (SD $\cong$ 1.7 N) with an average error of 12.1%.**

***Index Terms*—Force, human–object interface, MEMS, sensor, shear, silicon.**

I. Introduction

FORCES distributed at the skin–object interface are of strong interest and importance in areas such as biomechanical modeling, clinical evaluations, and rehabilitation devices. One example is the palmar force distribution during grip functions. Conventional methods for measuring exertion levels during grasping activities include subjective magnitude estimation, electromyography and direct instrumentation of objects. Magnitude estimation is relatively low in resolution and depends on the objectivity of the participant. Surface electromyography has been used for studying power gripping, pinching, and precision handling at different exertion levels [1]. Force measurement using the surface electromyography, however, is mainly limited to static exertions, fixed postures, and specificity of individual fingers. Accurate predication of internal hand forces using biomechanical models has been limited because adequate force sensors have not been available for measuring individual finger and hand forces during gripping activities. Force sensors are needed for postsurgical evaluation in procedures such as joint replacement and tendon transfers. Accurate, reliable force sensors are also needed for use with functional neuromuscular stimulation (FNS) [2]. In addition, shear force is believed to be a cause of the formation of the pressure sores in wheelchair bound subjects and the plantar ulcer development in individuals with diabetes mellitus [3]. The estimated annual national cost for hospitalization and patient care due to such ulcerations approaches $1 billion [24]. Attempts to isolate or describe these effects have been limited because no suitable sensors are available. In all of the above applications, the measurement of both the normal and shear components of an applied load would be beneficial.

Many types of normal force sensors [4]–[14] and a few shear sensors (discussed below) have been developed via a variety of transduction methods for use in robotics, industry, and medicine [15]. Compared with measuring pressure or normal force, measuring shear force can be challenging. While several fluid shear micro sensors have been developed, only a few shear sensors have been developed for measuring mechanical shear forces. Kane and Kovacs [16] reported a point-traction shear-stress-sensitive sensor. The device was composed of a central shuttle plane suspended over a cavity by four bridges. Four polysilicon peizoresistive elements were embedded in each of the bridges as strain gauges. The shear and normal stress components of an applied traction stress were determined by measuring the four bridge node voltages in a sensor resistor network. Jin and Mote [17] reported a sensor with a similar structure but using a suspended polysilicon crossbeam. Twelve piezoresistors were connected into three Wheatstone bridges for resolving three force components. Jiang *et al.* [18] developed a polyimide-packaged shear-stress sensor skin used for measuring the wall shear stress exerted by viscous flow for aerodynamics study. Yao [19] integrated eight piezoresistors into a boss-diaphragm structure to make a shear-force sensor. Four resistors were placed on the X axis and four others were placed on the Y axis. Four resistors on each axis were connected into a Wheatstone bridge. In order to sense a shear force, the compression and tension of the resistors on the same axis were required to be equal. All eight resistors were required to be identical. However, symmetrical deformation is unlikely in practice since the resistors are located neither in the middle plane nor at the center of the diaphragm.

We recently developed a silicon-based shear-sensitive micro sensor. The sensor's design, fabrication, modeling, and characterization (bench tests) were published in [20]. The bench testing results showed that the sensor was capable of measuring both the normal and shear components of a mechanically applied force. In order to apply the sensor to human–object interface studies, we further investigated the sensor's behavior in response to human hand forces. In this paper, the design and fab-

Manuscript received June 18, 2001; revised April 21, 2002. This work was supported by the Whitaker Foundation. *Asterisk indicates corresponding author.*.

L. Wang is with Texas Instruments Incorporated, and also the Department of Electrical and Computer Engineering, The Beckman Institute for Advanced Science and Technology, University of Illinois, Urbana, IL 61801 USA.

*D. J. Beebe is with the Department of Electrical and Computer Engineering, The Beckman Institute for Advanced Science and Technology, University of Illinois, Urbana, IL 61801 USA, and also the Department of Biomedical Engineering, University of Wisconsin, 1410 Engineering Dr., Madison 53706 USA (e-mail: dbeebe@engr.wisc.edu).

Digital Object Identifier 10.1109/TBME.2002.804586

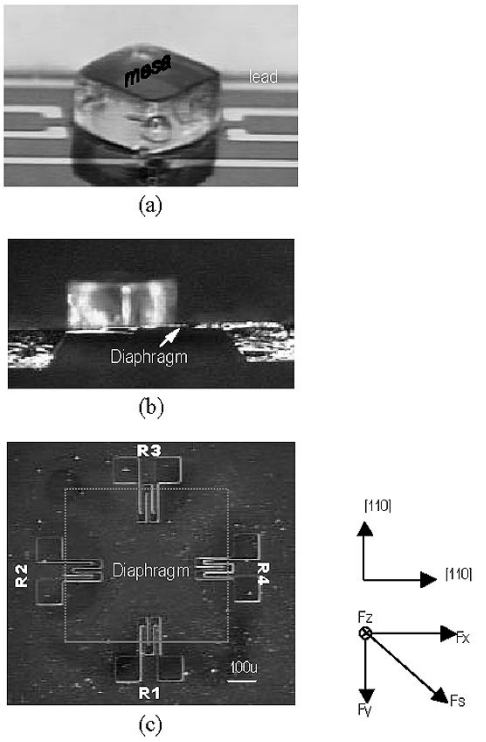

Fig. 1. Pictures of a sensor. (a) Perspective view shows the whole structure of the sensor, and resistors' location with respect to mesa. (b) Cross-sectional view shows silicon diaphragm and cavity. (c) Top view (of the sensor prior to leads or mesa) shows the resistor layout.

rication of the sensor are briefly reviewed. The methods of sensitivity calibration and force measurement are described. The characterization results of the sensor under 5- to 40-N shear force and 0- to 30-N compressive forces of grasping are presented. The shear-force measurement is discussed.

II. Sensor Design and Fabrication

Referring to Fig. 1, the sensor is a silicon diaphragm structure instrumented with four piezoresistors. A square mesa on top of the diaphragm is used to convert an applied force to stress. In order to determine three directional components of a load, (at least) three independent sensing elements are needed. In this design, each of the four piezoresistors works as an independent gage. They are placed under the bottom corners of the mesa and in the middle of the diaphragm edges for an increased sensitivity. The length of the resistor is much greater than the width for an increased measurement accuracy. As a force is applied, the diaphragm is deformed. The resulting stresses induced in the resistors lead to resistance changes. In particular, for a nonnormal load (i.e., a load with both normal and shear components), an asymmetric stress distribution is generated in the diaphragm. By measuring the resistance change of each resistor in response to the load, one can resolve both compressive and shear components of the force. Detailed discussions regarding the resistors' orientation type, size, and location; force transmission mesa; and sensor's model are described in the previous work [20].

The sensor was fabricated using integrated circuit fabrication and microelectromechanical technologies. Two wafers are used. The diaphragm is formed by creating a cavity in the top (sensing) wafer via the KOH etching. The cavity is sealed by bonding the sensing wafer to another substrate (bottom) wafer for an increased sensitivity via more rigid boundary conditions leading to higher stress levels in the resistors. The piezoresistors are created via Boron implantation. Leads are made in polyimide/Aluminum/polyimide sandwich structure and can be released to realize a flexible leads. The square mesa is made of EPON SU-8 (super-thick photoresist via photolithography process).

III. Characterization Method

Hand forces of (0–40 N) were used for the sensor's characterization when subjects were performing grasp and lifting. The characterization of the sensor on subjects consists of two steps: calibration of the sensitivities, and force measurement. The normal sensitivity was calibrated when only a compressive force was applied whereas the shear sensitivity was calibrated with both shear and compressive forces applied. Force measurement was performed via a tracking experiment at different levels of compressive and shear forces. In this section, the methods of the calibration and force measurement are discussed. The experimental will be described in Section IV.

A. Calibration of Sensitivities

An applied force ($\mathbf{F}$) can be decomposed into three orthogonal components with respect to the resistor orientation, namely, $F_{//}$, $F_{\perp}$, and F_n. $F_{//}$, $F_{\perp}$ are longitudinal and transversal shear components that are parallel and perpendicular to the length of the resistor, and F_n is the normal component that is perpendicular to the resistor's top surface. The total resistance change of a resistor is contributed by each of these three components, and thus can be expressed as the linear combination of the force components [20]

$$\frac{\Delta R}{R} = k_{//}F_{//} + k_{\perp}F_{\perp} + k_n F_n \tag{1}$$

where

$$\begin{cases} k_n = \frac{1}{2}\pi_{44}(k_{//,n} - k_{\perp,n}) \\ k_{//} = \frac{1}{2}\pi_{44}(k_{//,//} - k_{\perp,//}) \\ k_{\perp} = \frac{1}{2}\pi_{44}(k_{//,\perp} - k_{\perp,\perp}). \end{cases} \tag{2}$$

In (2), π_{44} is the piezoresistive coefficient. $k_{i,j}$ ($i, j = //$ or $\perp$) is a proportionality coefficient related to Young's modulus, shear modulus, and Poisson's ratio of silicon and EPON su-8 resist, and size and geometry of the diaphragm and mesa. If the coefficients k_j ($j = n, //, \perp$) are invariant with applied force, the normal, and shear sensitivities S_n, $S_{//}$, $S_{\perp}$ can be expressed by

$$\begin{cases} S_n \equiv \left.\dfrac{\partial(\Delta R/R)}{\partial F_n}\right|_{\substack{F_{//}=0 \\ F_{\perp}=0}} = k_n \\ S_{//} \equiv \left.\dfrac{\partial(\Delta R/R)}{\partial F_{//}}\right|_{\substack{F_n=0 \\ F_{\perp}=0}} = k_{//} \\ S_{\perp} \equiv \left.\dfrac{\partial(\Delta R/R)}{\partial F_{\perp}}\right|_{\substack{F_n=0 \\ F_{//}=0}} = k_{\perp} \end{cases} \tag{3}$$

where "≡" represents the definition. Normal sensitivity S_n can be calibrated by measuring the resistance change when only compressive force is applied. For the shear sensitivity ($S_{\perp,}$ or $S_{//}$), however, considering that both shear and compressive forces are exerted at the same time in the human hand griping activities, the shear sensitivity calibration was performed when both compressive force F_n and shear force ($F_{//}$ or $F_{\perp}$) were applied. By subtracting the resistance change contributed by the compressive force from total resistance change measured, the resistance change due to the shear component is obtained. Using (2) and (3), the shear sensitivities can be rewritten as shown in (4) together with the normal sensitivity

$$\begin{cases} S_n = \dfrac{\Delta R/R\big|_{\substack{F_{\perp}=0 \\ F//=0}}}{F_{//}} = k_n \\ S_{//} = \dfrac{\Delta R/R\big|_{F_{\perp}=0} - S_n F_n}{F_{//}} \\ S_{\perp} = \dfrac{\Delta R/R\big|_{F_{\perp}=0} - S_n F_n}{F_{\perp}} \end{cases} \tag{4}$$

where $(\Delta R/R)_{F//=0,\,F\perp=0}$ is the resistance change in response to compressive force, whereas $(\Delta R/R)_{F\perp=0}$, represents the resistance change due to both longitudinal shear and compressive forces, and $(\Delta R/R)_{F//=0}$ means the resistance change due to both transversal shear and compressive forces.

B. Force Measurement

With calibrated sensitivities and measured resistance change for each resistor, namely, $S_{n,\,j}$, $S_{//,\,j}$, and $S_{\perp,\,j}$; and $\Delta R_j/R_j$ ($j = 1, 2, 3, 4$ here denoting resistor number), the three components of an applied force F_x, F_y, and F_z, (referring to Fig. 1 for the definition of the force directions) can be obtained by solving any three equations in

$$\begin{cases} \dfrac{\Delta R_1}{R_1} = S_{\perp,1}F_x + S_{//,1}F_y + S_{n,1}F_z \\ \dfrac{\Delta R_2}{R_2} = S_{//,2}F_x + S_{\perp,2}F_y + S_{n,2}F_z \\ \dfrac{\Delta R_3}{R_3} = S_{\perp,3}F_x + S_{//,3}F_y + S_{n,3}F_z \\ \dfrac{\Delta R_4}{R_4} = S_{//,4}F_x + S_{\perp,4}F_y + S_{n,4}F_z \end{cases} \tag{5}$$

where $S_{i,\,j}$ ($i = \perp, //, n$; $j = 1, 2, 3, 4$) can be of positive or negative value depending on the direction of the applied force with respect to each resistor. In our experiment, we aligned the shear force in parallel to the length of a resistor. Then (5) can be simplified with F_x equal to zero

$$\begin{cases} \dfrac{\Delta R_1}{R_1} = S_{//,1}F_s + S_{n,1}F_n \\ \dfrac{\Delta R_2}{R_2} = S_{\perp,2}F_s + S_{n,2}F_n \\ \dfrac{\Delta R_3}{R_3} = S_{//,3}F_s + S_{n,3}F_n \\ \dfrac{\Delta R_4}{R_4} = S_{\perp,4}F_s + S_{n,4}F_n. \end{cases} \tag{6}$$

Theoretically, two equations above corresponding any two adjacent resistors are sufficient to resolve the F_s and F_n. For example, using R_1 and R_2

$$\begin{cases} F_n = \dfrac{S_{//,1}\frac{\Delta R_2}{R_2} - S_{\perp,2}\frac{\Delta R_1}{R_1}}{S_{//,1}S_{n,2} - S_{\perp,2}S_{n,1}} \\ F_s = \dfrac{S_{n,2}\frac{\Delta R_1}{R_1} - S_{n,1}\frac{\Delta R_2}{R_2}}{S_{//,1}S_{n,2} - S_{\perp,2}S_{n,1}}. \end{cases} \tag{7}$$

In the experiments, however, the resistance changes of all four resistors were measured as shear force was applied parallel to their length.

IV. Experimental

The sensitivity calibration was performed when (0–30 N) compressive force and (5–40 N) shear force were applied. The tracking experiment was performed at three compressive force levels (7, 15, and 26 N) and four shear-force levels (9, 18, 25, and 35 N). The sensor was tested on six subjects. Each measurement was repeated six times. In this section, the testing system and testing results are described.

A. Testing System

The experimental system consists of a dynamometer based loading structure, signal conditioning, data acquisition, and data analysis. The loading structure is shown in Fig. 2. The sensor was mounted on one arm of a dual beam strain gage dynamometer [21] that was used to measure the compressive force applied on the sensor. The dynamometer was calibrated prior to the sensor testing. Weights were attached to the base of the dynamometer to create a shear load orthogonal to the compression. Each of the four resistors was connected into a separate off-sensor Wheatstone bridge. The output of each Wheatstone bridge, along with the dynamometer output, were amplified (gain = 500) and sampled (30 Hz) through five 12-bit analog–digital converter channels.

B. Calibration of Sensitivity

The calibration of normal and shear sensitivities was performed on six subjects over a shear loading range of 5- to 40-N at increments of 1.25 N. At each shear loading, the subjects were instructed to lift the dynamometer, gradually pinch up to a 30-N compressive force and then slowly release (For the normal sensitivity calibration, the dynamometer was kept stationary on a table, i.e., pinch only without lifting). Each measurement was repeated six times. Fig. 3 shows a typical pinch-induced sensor output in response to the pinch/release force (no shear loading). In order to express the variation of shear-induced output with its corresponding shear loading (shear sensitivity is not constant as discussed in Section V-C), as discussed in Section III-A, we subtracted the pinch force output from the total output and obtained the pure shear-induced output at all pinch levels (The 0∼30-N pinch force was digitized as 60 discrete levels at the incremental of 0.5 N). Fig. 4 plotted a typical shear-induced output varying with the shear loading at a single pinch level of 20 N. The slopes of the curves in Fig. 3 represent the normal sensitivity for each resistor, whereas the slopes of the curves in

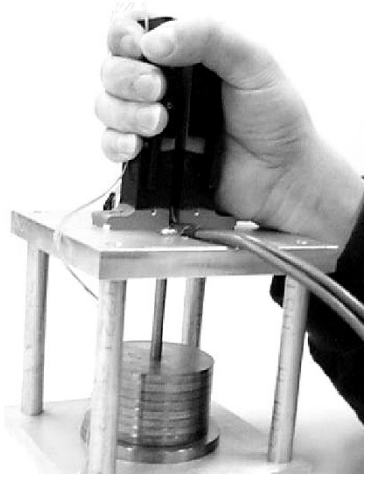

(a)

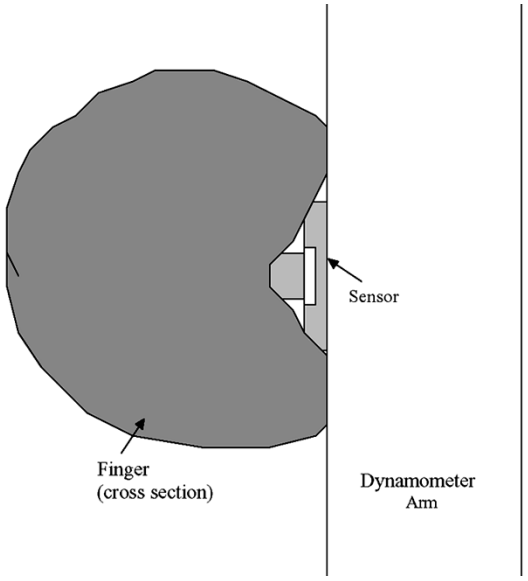

(b)

Fig. 2. Loading setup—(a) Sensor is mounted on dynamometer. Compressive force is applied via pinching the dynamometer beams, while the shear force is applied by attaching the weights on the base of the dynamometer. (b) Interface between finger and dynamometer at sensor's location shows that portion of pinch force is bypassed.

Fig. 4 (more strictly, the derivatives at each shear loading) represent the shear sensitivities.

C. Tracking Experiment

To evaluate the sensor's performance of force measurement, a tracking experiment was performed at four shear-force levels (9,18, 25, and 35 N). At each shear level, the subjects were asked to pinch the dynamometer to a specific level, hold at that level for approximately 2 s and release the pinch. Three pinch levels (7, 15, and 26 N) were used. Visual force feedback was provided to the subjects on the computer monitor. A run consisted of five consecutive pinch/hold/release patterns for each pinch level. Each run was repeated six times. This tracking experiment was performed for each resistor by rotating the sensor attachment by 90° each time. Fig. 5 shows a typical sensor and dynamometer response. Using the calibrated sensitivities (4) and(7), the shear forces were calculated for each loading and

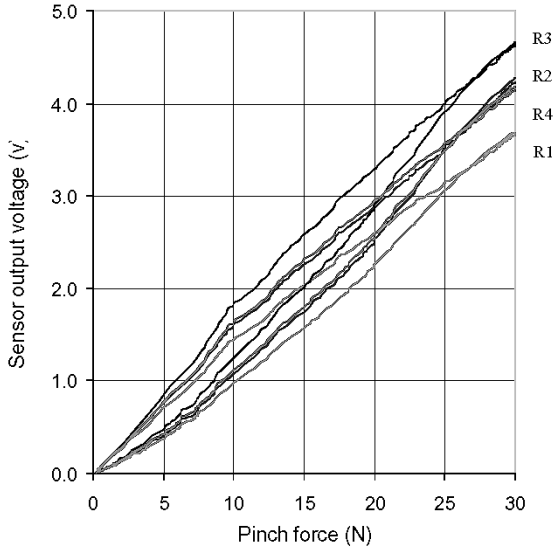

Fig. 3. Compression-induced voltage versus compressive force applied. The slopes of the curves are normal sensitivities of the resistors.

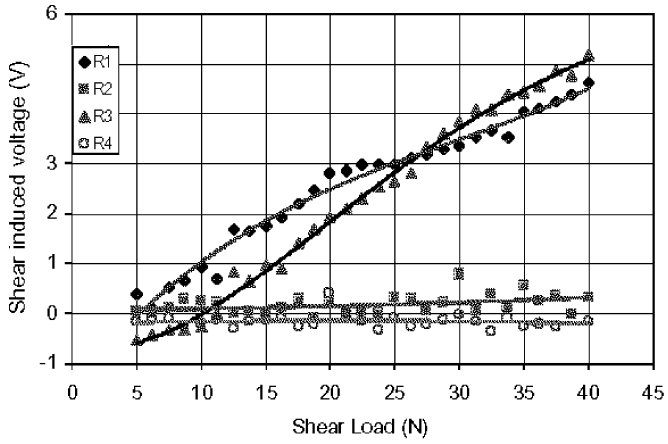

Fig. 4. Shear-induced output versus shear load nonlinearly shows that shear sensitivity is not a constant (at the pinch force of 20 N).

each subject, and averaged over six measurements and four resistors. Their mean values and standard deviations are listed in Table I. Compared with the actual shear loading, the measurement errors are calculated and listed in Table II. The mean values and errors are then averaged over six subjects. Figs. 6 and 7 plot the averaged results, respectively.

V. Discussion

The experimental results showed that the sensor is sensitive to human hand forces and is capable of measuring both the normal and shear forces at skin–object interface. The discussion includes the sensing ability, force measurements, and deviations. Shear sensitivity and shear-force measurement are mainly discussed.

A. Compressive Force Sensing Ability

Fig. 5 shows that the sensor is sensitive to human hand forces. As shown in Fig. 3, the normal sensitivity varies little over the pinch force of 0- to 30-N (The hysteresis will be discussed

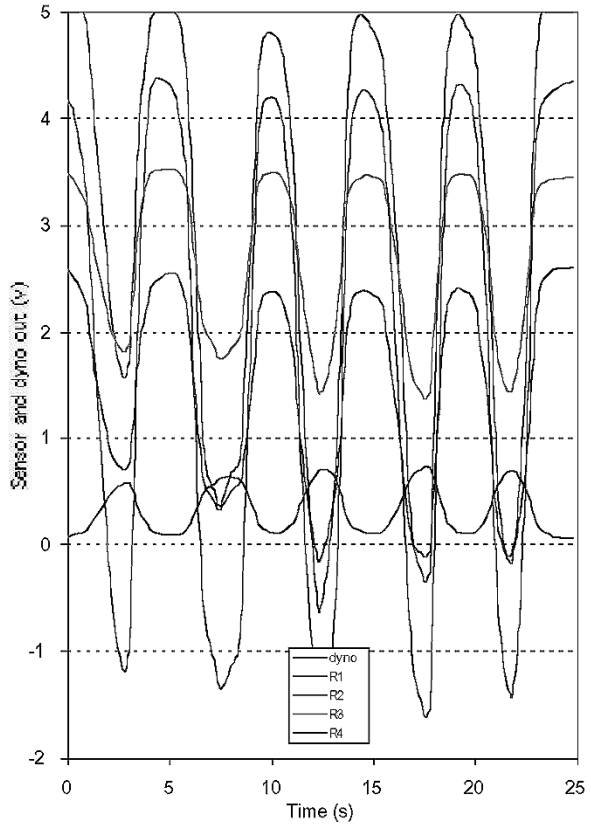

Fig. 5. Typical sensor and dynamometer response in tracking experiment.

below). The result indicates that the normal sensitivity is independent of the compressive force. In general, the normal sensitivity depends upon the thickness and size of the diaphragm, the location of the resistors with respect to the diaphragm edges, and the mesa corners. The thinner the diaphragm, the higher the sensitivity. The closer the resistor is to the diaphragm edge, the higher the sensitivity. However, there is a minimum thickness of the diaphragm (relevant to the diaphragm area) required by the maximum load. Some diaphragm protection technique such as bottom-up protection was used in previous work [5]. All these geometric sizes and relevant positions, if going down very small, like in the scale of submicrometer, will be limited by the fabrication tolerances. From Fig. 3, one can see some deviation in normal sensitivity among the resistors. The deviation may be caused by the nonuniform (compressive) force application over the mesa top surface.

B. Shear-Force Sensing Ability

Referring to Fig. 4, since R_2 and R_4 are perpendicular to the shear loading and their width is much smaller than their length, the induced longitudinal and transverse stresses (parallel and perpendicular to the resistor length) are both small leading to little response to the shear force. On the other hand, since R_1 and R_3 are parallel to the shear loading direction, significant changes of their resistances with the shear force are observed. These changes imply that the sensor is sensitive to the shear loading. These shear-induced voltages, however, vary in nonlinear fashion with the shear load as discussed below.

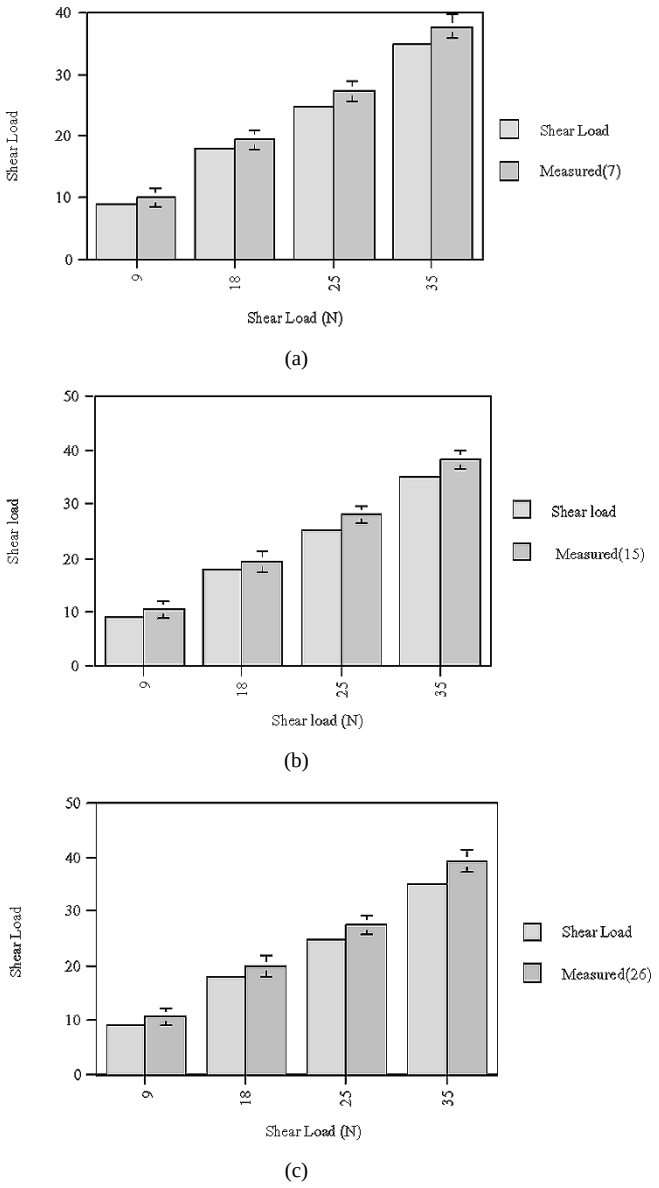

Fig. 6. Measured shear forces (averaged for all six subjects) are plotted together with the actual shear loadings at different pinch level of (a) 7, (b) 15, and (c) 26 N. Error bars represent standard deviation of the measured shear forces.

C. Nonlinearity

Nonlinearity was observed only in the case of shear-force application (The hysteresis is ignored here and will be discussed below). It is originated from the nonlinear transitions from shear force to the induced stress in the diaphragm, which happens at hand/sensor interface, and mesa/diaphragm interface.

In contrast to the pinch-only case (Fig. 3) where the stresses induced in the resistors are linearly proportionally to the applied compressive force (approximately in a factor of the area of the mesa base), the shear induced stress (Fig. 4) changes nonlinearly with the shear force since the shear force is applied in the direction parallel to the sensor surface. In addition to depending on the shear force, the shear induced stress also depends on the relative amount of the shear loading to the compressive force, the mesa structure, and the size of the diaphragm.

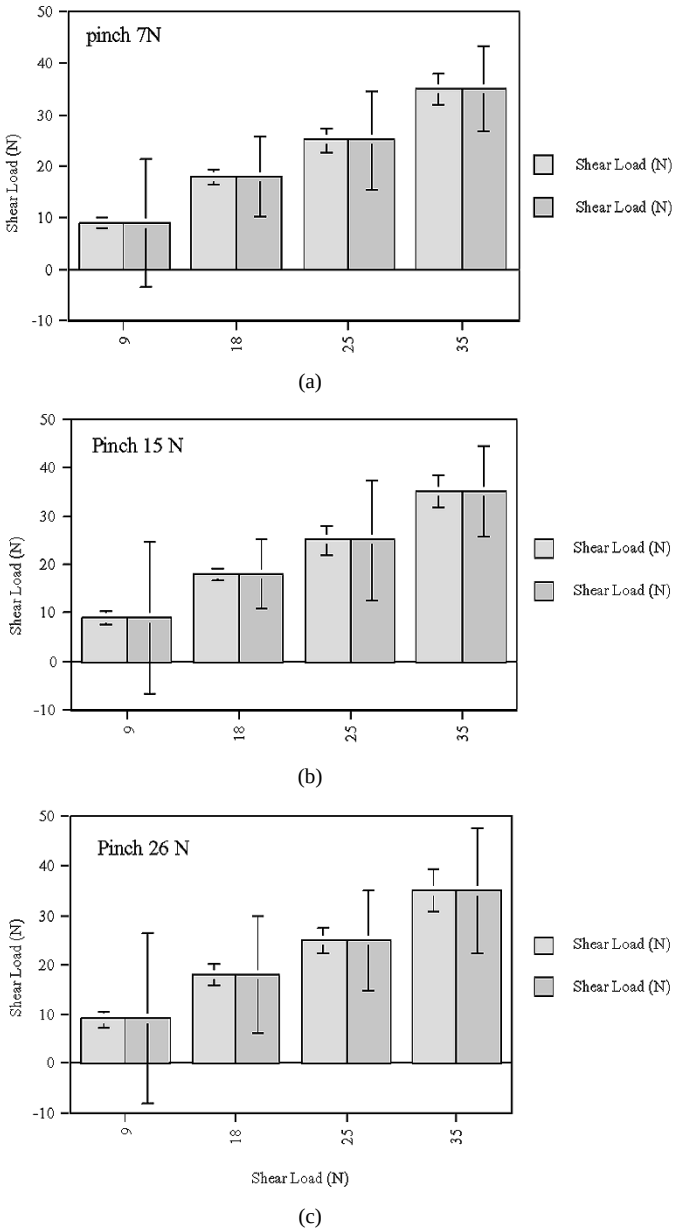

Fig. 7. Errors between the actual and measured shear load (averaged for all six subjects) for different shear loadings in terms of pinch levels of (a) 7, (b) 15, and (c) 26 N. Left error bars represent actual errors and right error bars represent percent error.

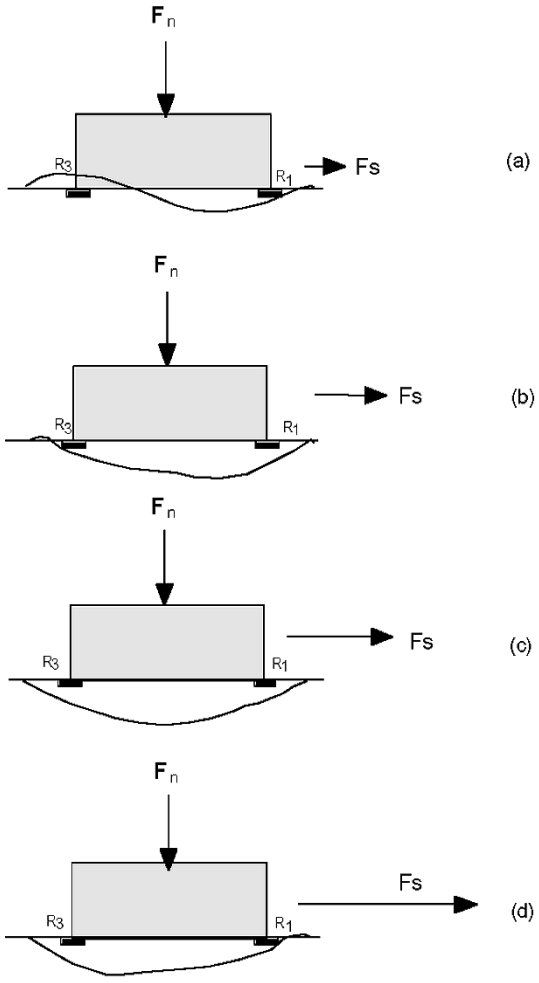

Fig. 8. Schematic illustration of shear-induced diaphragm deformations for different shear loadings at a pinch force of 20 N: (a) $Fs < 10$ N; (b) $10\ N < Fs < 27$ N; (c) $Fs = 27$ N; and (d) $Fs > 27$ N.

We have previously performed the finite element modeling on the force sensors where the sensor–skin/tissue interface was not included [22], [23]. The modeling of the complete skin/sensor system, however, is nontrivial. Similar to the nonlinearity analysis for the bench testing [20], here we use the stresses induced in the resistors to explain the variation of the shear-induced resistance with the shear load in a relative qualitative manner. Referring to Fig. 8(a), when the shear force is small relative to the pinch force ($Fs < 10$ N, pinch $= 20$ N), a tension is induced in R_3 resulting in a negative voltage output (as shown in Fig. 4). As the shear force increases, the tension in R_3 decreases and transitions into compression [Fig. 8(b)]. The difference between the shear-induced output of R_1 and R_3 becomes smaller. When the shear force is about 27 N, this difference becomes zero. This means that the stresses induced in both resistors ar equal, as illustrated in Fig. 8(c). As the shear increases further, more compression is induced in R_3, resulting in a larger output voltage observed across R_3 than across R_1 as illustrated in Fig. 8(d) and shown in the high shear region of $Fs > 27$ N in Fig. 4.

D. Hysteresis

The performance of the sensor in subject testing is degraded as compared with the bench testing results. Referring to Fig. 3, the maximum hysteresis of ∼8% relative to the expected full-scale voltage was observed as compared with only 2.5% in bench testing. The performance degradation in hysteresis is caused by the viscoelastic nature of the human skin and soft tissue.

E. Shear-Force Measurement

The experimental results show that the sensor has good accuracy and repeatability for shear-force measurements. For shear loads of 9- to 35-N and a pinch force of 7–26 N, the absolute shear measurement error falls in the range of −1.39- to 4.49-N (see Table II). The percent error falls between 6.7%–19.4%, and the average percent error is 12.1%. The data listed in Table I

TABLE I
MEASURED SHEAR FORCE AND STANDARD DEVIATION AT VARIOUS PINCH LEVELS (N)

Subject# (sex, age)	Shear load (N)	Pinch Level 7N	Pinch Level 15N	Pinch Level 26N
1 (M,36)	9	9.85 (1.34)	10.03 (1.35)	10.43 (1.28)
	18	19.39 (1.78)	19.65 (1.98)	19.95 (1.86)
	25	26.45 (1.54)	28.05 (1.24)	27.83 (1.75)
	35	37.58 (1.67)	38.06 (1.56)	38.86 (2.04)
2(M, 31)	9	9.59 (1.54)	10.98 (1.47)	10.17 (1.64)
	18	18.59 (1.69)	18.78 (2.09)	20.65 (1.44)
	25	27.03 (1.99)	27.83 (1.95)	29.43 (1.91)
	35	37.87 (2.12)	37.76 (1.78)	39.36 (1.86)
3(F, 36)	9	10.43 (1.66)	9.94 (1.43)	10.29 (1.69)
	18	19.06 (1.39)	19.52 (1.75)	21.28 (1.98)
	25	28.02 (1.13)	28.66 (1.54)	28.07 (1.63)
	35	37.45 (1.66)	39.49 (1.84)	38.96 (2.82)
4(F, 28)	9	10.55 (1.79)	11.04 (1.69)	10.66 (1.28)
	18	20.36 (1.46)	20.35 (1.50)	21.00 (1.84)
	25	27.33 (2.02)	28.64 (1.59)	28.18 (1.77)
	35	38.21 (1.75)	38.46 (1.57)	40.30 (1.94)
5(M, 34)	9	10.33 (1.40)	10.45 (1.60)	11.34 (1.66)
	18	19.46 (1.33)	18.53 (2.03)	21.33 (2.00)
	25	27.87 (1.21)	28.12 (1.44)	27.21 (1.45)
	35	38.11 (1.55)	37.33 (1.78)	39.43 (1.86)
6(F, 33)	9	9.90 (1.21)	10.03 (1.45)	10.43 (1.40)
	18	19.45 (1.56)	18.78 (2.00)	16.61 (1.89)
	25	27.57 (1.36)	27.05 (1.56)	24.31 (1.59)
	35	38.04 (1.89)	38.56 (1.99)	39.30 (1.93)

TABLE II
ERROR BETWEEN ACTUAL AND MEASURED SHEAR FORCE AT VARIOUS PINCH LEVELS (N)

Subject # (sex, age)	Shear Load (N)	Pinch Level 7N	Pinch Level 15N	Pinch Level 26N	Average Error (%)
1 (M,36)	9	0.85	1.03	1.43	12.26
	18	1.39	1.65	1.95	9.24
	25	1.45	3.05	2.83	9.77
	35	2.58	3.06	3.86	9.05
2(M, 31)	9	0.59	1.98	1.17	13.85
	18	0.59	0.78	2.65	7.44
	25	2.03	2.83	4.43	12.39
	35	2.87	2.76	4.36	9.51
3(F, 36)	9	1.43	0.94	1.29	13.56
	18	1.06	1.52	3.28	10.85
	25	3.02	3.66	3.07	13.00
	35	2.45	4.49	3.96	10.38
4(F, 28)	9	1.55	2.04	1.66	19.44
	18	2.36	2.35	3.00	14.28
	25	2.33	3.64	3.18	12.20
	35	3.21	3.46	5.3	11.40
5(M, 34)	9	1.33	1.45	2.34	18.96
	18	1.46	0.53	3.33	9.85
	25	2.87	3.12	2.21	10.93
	35	3.11	2.33	4.43	9.40
6(F, 33)	9	0.90	1.03	1.43	12.44
	18	1.45	0.78	-1.39	6.70
	25	2.57	2.05	-0.69	9.83
	35	3.04	3.56	4.30	10.38
					Total avg error **12.10%**

show an average standard deviation of ~1.77 N over the shear-force range of 9 to 35 N.

As shown in Fig. 7, typically, the absolute measurement error (left error bars) increases as both the pinch level and shear loading increase. The percent error (right error bars), however, decreases as shear loading increases from 9 to 18 N and then remains relatively constant with further increases in shear load. Since the mesa is much smaller than the thumb, as the applied force increases, the mesa begins to sink into the thumb, causing a portion of the force to bypass the sensor [refer to Fig. 2(b)]. Thus, the higher the load, the more force is bypassed, resulting in increased absolute measurement error. On the other hand, relative to the shear load, the bypass phenomena is significant at small shear value and tends to be "saturated" at high shear level. From Table II, one can see that the measurement error varies from subject to subject. For example, the error present in subject 4 is larger than that in subject 1. These differences may be due to the different mechanical characteristics of the thumbs of different subjects. More subjects and further study are needed to quantify these effects.

VI. CONCLUSION

While numerous pressure and force sensors have been developed, no small unobtrusive shear-force-sensitive sensor is available for human–object interface studies. In this paper, we describe a shear-sensitive force sensor and its application to measuring compressive and shear forces at the skin–object interface. The sensor was calibrated on human subjects with a 5- to 40-N shear force and a 0- to 30-N compressive force. Good repeatability (SD $\cong$ 1.7 N) and good accuracy (average error between the actual and the measured shear load $\cong$ 12.1%) were observed. Currently, an array of such sensors is being mounted on a tool for investigating the human hand's behavior during grasping activities.

REFERENCES

[1] T. J. Armstrong, D. B. Chaffin, and J. A. Foulke, "A methodology for documenting hand positions and forces during manual work," *J. Biomech.*, vol. 12, pp. 131–133, 1979.
[2] P. E. Cargo, H. J. Chizeck, M. R. Neuman, and T. F. Hambrecht, "Sensors for use with functional neuromuscular stimulation," *IEEE Trans. Biomed. Eng.*, vol. BME-33, pp. 256–257, 1986.
[3] A. M. Labar, G. F. Harris, J. J. Wertsch, and H. Zhu, "An optoelectric planar 'shear' sensing transducer: Design, validationm and preliminary subject tests," *IEEE Trans. Rehab. Eng.*, vol. 4, pp. 310–319, Dec. 1996.
[4] T. R. Jensen, R. G. Radwin, and J. G. Webster, "A conductive polymer sensor for measuring external finger forces," *J. Biomech.*, vol. 24, pp. 851–858, 1991.
[5] D. J. Beebe, D. D. Denton, R. G. Radwin, and J. G. Webster, "A silcon-based tactile sensor for finger-mounted applications," *IEEE Trans. Biomed. Eng.*, vol. 45, pp. 151–159, Feb. 1998.
[6] T. A. Chase and R. C. Luo, "A capacitive tri-axial tactile force sensor design," in *Proc. EEE/ASME International Conf. Advanced Intelligent Mechatronics'97*, New York, p. 58.
[7] D. Spaldonova, J. Suriansky, and M. Nevesely, "Tactile force and spatial location measurement using ultrasonic transducers," *J. Elect. Eng.*, vol. 47, pp. 254–257, 1996.
[8] S. Akayama, C. Peng, T. Matsumiya, and T. Toyota, "Development of double-octagon tactile sensor for grasping control," in *Proc. IEEE/ASME Int. Conf. Advanced Intelligent Mechatronics*, Atlanta, GA, 1999, pp. 434–439.

[9] T. Mei, Y. Ge, Y. Chen, L. Ni, W.-H. Liao, Y. Xu, and W. J. Li, "Design and fabrication of an integrated three-dimensional tactile sensor for space robotic applications," in *Proc. IEEE Int. MEMS 99 Conf./12th IEEE Int. Conf. Micro Electro Mechanical Systems*, Orlando, FL, 1999, pp. 112–117.
[10] K. Nakamura and M. Uchiyama, "A fiber optic vertical coupler for the matrix tactile sensor," *Trans. Inst. Elect. Eng. Japan*, pt. A, vol. 119-E, pp. 113–114.
[11] P. Li and Y. Wen, "An arbitrarily distributed tactile-sensor array based on a piezoelectric resonator," *Int. J. Robot. Res.*, vol. 18, pp. 152–158, 1999.
[12] O. Lindahl, S. Omata, and K.-A. Angquist, "A tactile sensor for detection of physical properties of human skin *in vivo*," *J. Med. Eng. Technol.*, vol. 22, pp. 147–153, 1998.
[13] Y. Yamada, M. Nishigaki, S. Huang, and Y. Umetani, "Development of dynamic tactile sensor elements independently distributable on a compliant skin," *Trans. Soc. Instrum. Contr. Eng.*, vol. 34, pp. 275–277, 1998.
[14] H. Shinoda, K. Matsumoto, and S. Ando, "Tactile sensing based on acoustic resonance tensor cell," in *Proc. Tranducers 97: Int. Conf. Solid-State Sensors and Actuators*, Chicago, IL, pp. 129–132.
[15] J. G. Webster, *Preventing Pressure Sores*. New York: Wiley, 1991.
[16] B. J. Kane and G. T. A. Kovacs, "A CMOS compatible traction stress sensing element for use in high resolution tactile imaging," in *Proc. Transducers'95*, Stockholm, Sweden, pp. 648–651.
[17] W. L. Jin and C. D. Mote, "Development and calibration of a sub-millimeter three-component force sensor," *Sensors Actuators A*, vol. 65, pp. 88–94, 1998.
[18] F. Jiang, Y. Tai, K. Walsh, T. Tsao, G. Lee, and C. Ho, "A flexible MEMS technology and its first application to shear stress sensor skin," in *Proc. IEEE MEMS'97*, pp. 465–470.
[19] C. T. Yao, M. C. Peckerar, J. H. Wasilik, C. Amazeen, and S. Bishop, "A novel three-dimensional microstructure fabrication technique for a triaxial tactile sensor array," in *Proc. IEEE Micro Robots and Teleoperators Workshop*, 1987, pp. 41–46.
[20] L. Wang and D. J. Beebe, "A silicon-based shear force sensor: Development and characterization," *Sensors Actuators A*, vol. 84, pp. 33–44, 2000.
[21] R. G. Radwin, G. P. Masters, and F. W. Lupton, "A linear force-summing hand dynamometer independent of point of application," *Appl. Ergonom.*, vol. 22, pp. 339–343, 1991.
[22] A. C. Costea, "Finite-element modeling of a fiber optic based silicon tactile shear sensor," Ph.D. dissertation, Dept. Biomed. Eng., Louisiana Tech. Univ., Ruston, May 1996.
[23] J. Garvey, D. J. Beebe, and D. D. Denton, "Finite element modeling of a silicon tactile sensor," *Sensors Mater.*, vol. 9, no. 5, 1997.
[24] M. E. Levin, "Saving the diabetic foot," *Med. Times*, vol. 108, p. 56, 1980.

Lin Wang received the B.S. degree in electrical engineering and the M.S. degrees in biomedical engineering from the Southeast University, Nanjing, China (1982 and 1988), the Interstate University of Applied Sciences in Switzerland (1990) and Louisiana Tech. University, Ruston (1996). He received the Ph.D. degree in electrical engineering from the University of Illinois at Urbana-Champaign in 2001.

From 1982 to 1994, he was with the Department of Biomedical Engineering at the Southeast University, where he was an Assistant/Associate Professor doing research in ultrasonic imaging, molecular electronics, and scanning tunneling microscopy. From 1994 to 1996, he was with Louisiana Tech. University, where he was a Research Assistant and developed new embryo labeling technologies. From 1996 to 2000, he was with the Beckman Institute for Advanced Science and Technology at the University of Illinois where he was a Research Assistant designing and fabricating MEMS devices and developed new shear-force-sensitive microsensors. Since March 2000, he has been with Texas Instruments Incorporated, Manchester, NH, doing Mixed Signal IC design and has completed two high-performance power management IC products. He has over 40 publications.

David J. Beebe (S'89–M'90) received the B.S., M.S.,and Ph.D. degrees in electrical engineering from the University of Wisconsin-Madison, in 1987, 1990, and 1994, respectively.

He is an Associate Professor in the Department of Biomedical Engineering, at the University of Wisconsin-Madison, with joint appointments in electrical and computer engineering and mechanical engineering. From 1996–1999, he was an Assistant Professor in the Department of Electrical and Computer Engineering and as Assistant Professor at Louisiana Tech. University, Ruston. From 1991–1994 David was a National Institutes of Health (NIH) Biotechnology Predoctoral Trainee. During that time, he spent three months at Medtronic developing hemodynamic concepts. He was an Electrical Engineer for Kimberly-Clark Corp. from 1987–1989 where he lead the packaging controls group. He has over 120 publications including four book chapters. He has served on many government advisory panels including the NRC's National Nanotechnology Initiative review panel. Dr. Beebe is a co-founder of Vitae LLC that is commercializing microfluidic systems for assisted reproduction and consults for various companies in the biotech and microfluidics field. He is an inventor on three issued patents and 13 pending patent applications. He has broad interests in biomedical instrumentation and the development and use of microfabricated devices for applications in medicine and for the study of biology. His current interests include technology development for the handling and analysis of biological objects, the development of nontraditional autonomous micro fluidic devices and systems, the study of cell and embryo development in microenvironments, the development of electrostatic and electrocutaneous haptic displays, and the development of tactile sensors

Dr. Beebe serves on the steering/program committees for the MicroTAS and Hilton Head conferences and was a founding co-chair of the Annual IEEE EMBS Special Topic Conference on Microtechnology, Medicine and Biology.